Indian Journal of Pure & Applied Physics
Vol. 53, May 2015, pp. 328-334

Electronic structure and cohesive properties of GaN

G Arora[a], H S Mund[b], V Sharma[b], N L Heda[c] & B L Ahuja[b,*]

[a]Department of Physics, Geetanjali Institute of Technical Studies, Udaipur 313 001, Rajasthan, India

[b]Department of Physics, University College of Science, M L Sukhadia University, Udaipur 313 001, Rajasthan, India

[c]Department of Pure and Applied Physics, University of Kota, Kota 324 005, Rajasthan, India

*E-mail: blahuja1961@gmail.com

Received 5 April 2013; revised 17 July 2014; accepted 7 January 2015

The first-ever Compton profile of GaN employing high energy (662 keV) γ-radiations from a ^{137}Cs source has been reported. To compare our experimental momentum densities, the Compton profiles and electronic properties using density functional theory within linear combination of atomic orbitals have also been computed. The nature of bonding in GaN is compared with its isoelectronic InN using equal-valence-electron-density profiles and Mulliken's population. To establish applicability of Compton scattering in computation of cohesive energy, the cohesive energy using the experimental and theoretical momentum densities has also been studied. The energy bands and density of states computed using DFT calculations are compared with the existing data.

Keywords: Nitride semiconductors, Electronic band structure, X-ray, Gamma-ray spectroscopy

1 Introduction

It is well known that Compton scattering technique yields information about the fundamental ground state electron momentum density $\rho(\mathbf{p})$. In this method, the double differential Compton scattering cross-section is related to the electron momentum distribution of the target materials[1]. In bulk materials, Compton scattering technique is valid when the energy transferred during the interaction is much larger than the binding energy of the electronic states involved.

The relation between the Compton profile, $J(p_z)$, and the $\rho(\mathbf{p})$ is given by:

$$J(p_z)=\int\int \rho(\mathbf{p})\, dp_x\, dp_y \qquad \ldots(1)$$

where p_z is the component of the electron's ground state momentum along the scattering vector (z-axis).Within the independent-particle model, the $\rho(\mathbf{p})$ is related to $\psi_j(\mathbf{r})$ which are the occupied one particle wave functions. Therefore, the Compton scattering study of materials is helpful in understanding their electronic structure and chemical bonding etc. The experimental Compton profiles are also useful in verification of density functional theory (DFT), because the accuracy of results obtained from the DFT calculations depends upon the approximate nature of exchange and correlation potentials.

Among the III-V nitride compounds, GaN has fascinating properties which are useful in short wavelength light emitting diodes, high temperature and high power devices[2]. In general, wurtzite (WZ) nitrides are wide band gap materials with direct optical transition, high ionicity, high bond strength and good thermal conductivity. zinc-blende (ZB) III-V nitrides show a lower energy gap than WZ nitrides and a higher saturated electron drift velocity. In spite of different electronic band structure calculations and experimental investigations for electronic properties[3,24], a consistent picture related to the band gaps, the position of *d* and N(2*p*) bands as well as the hybridisation of N(2*s*) with semi-core *d* states of Ga is lacking. This keeps a great interest and considerable attention in the electronic properties of GaN.

The purpose of present work is multi-fold, namely to (a) measure Compton profile of GaN at intermediate resolution (b) compute Compton profiles using LCAO-DFT calculations and compare them with the present measurement (c) check the relative nature of bonding of GaN and InN using experimental and theoretical equal-valence-electron-density profiles (d) compute the cohesive energy employing the electron momentum densities and (e) deduce the electronic properties of GaN and visualize the role of different kind of exchange and correlation potentials including hybridization of Hartree-Fock (HF) and DFT schemes (B3LYP).

2 Theory

The electronic structure (including momentum densities) using local density approximation (LDA) and generalized gradient approximation (GGA) within DFT and B3LYP using CRYSTAL03 code[25] have been computed. The exchange and correlation potentials suggested by von Barth-Hedin[26] and Perdew-Burke-Ernzerhof[27] for DFT-LDA and DFT-GGA computations have been used, respectively. In the B3LYP, the exchange correlation density functional energy involves the Becke's gradient correction[28] to the exchange and correlation functionals using prescription of Lee-Yang-Parr[29] and Vosko-Wilk-Nusair[30].

To compute the electronic properties of GaN, the all-electron Gaussian basis sets[31] for Ga and N were used. To improve the convergence of N (2*p*) and Ga (3*d*) potentials, the basis sets were energy optimized using BILLY software. For faster convergence of self-consistent-field cycles, the BRODYEN scheme[32] was applied for all the calculations. The cut-off threshold parameters for Coulomb and exchange integral evaluation have been set to default values[25]. The integration in the reciprocal space has been carried out on a grid of 256 ***k*** points in the irreducible Brillouin zone (BZ), generated by a Monkhorst-Pack shrinking factor of 12. For the WZ-GaN, the lattice parameters[33] were a = 3.190 Å and c = 5.189 Å. The lattice constant a for the ZB-GaN was taken to be 4.50 Å.

3 Experimental Details

In the present measurements, the ^{137}Cs source primarily for investigating the electron momentum density has been used. Some salient features of our 20 Ci ^{137}Cs Compton spectrometer[34] are as follows: The incident γ-rays of 662 keV were scattered through a mean angle of 160±0.6° from the polycrystalline samples. The high purity (99.9± %) sample of WZ-GaN (pellet) was kept in a perspex ampoule having very thin Mylar sheets on both the sides. The momentum resolution (Gaussian, full width at half maximum), which includes the detector resolution and the geometrical broadening of the incident and the scattered photons was 0.38 au (1 au of momentum = 1.9929×10^{-24} kg m s^{-1}). The raw Compton data were corrected for background, instrumental resolution, Compton scattering cross-section and multiple scattering[1,34], etc. It may be noted that the instrumental resolution correction was limited to stripping off the low energy tail from the data, therefore, the theoretical profiles have to be convoluted with the instrumental resolution. The sample dimensions along with other experimental parameters are given in Table 1.

4 Results and Discussion

4.1 Energy bands and DOS

4.1.1 ZB structure

Energy bands of the ZB-GaN along with total and partial density of states (DOS) obtained using the DFT-GGA scheme within LCAO method are shown in Fig. 1. Due to a similar topology of energy bands and DOS (except some fine structure and band gap) within the DFT-LDA and the B3LYP schemes of LCAO, these bands are not shown here. Figure 1 shows that GaN in the ZB phase has a direct band gap at the Γ point. It is seen that the lowest valence bands originate due to mixing of the valence *d* electrons of Ga and the N (2*s*) states. The valence *d* bands are found to be highly resonant with the N (2*s*) bands. It is noticed that this pronounced mixing comes from both the segments of N (2*s*) bands lying above and below the valence *d* bands. From the DOS curves, it is seen that the upper valence bands in GaN are dominated by N (2*p*) states. Presently calculated band gaps are found to be 2.48, 2.46 and 3.58 eV at the Γ point for LDA, GGA and B3LYP, respectively. These values are compared with the available theoretical and the experimental data[3-6,9-11,14,15,18,19] as tabulated in Table 2. We find that for ZB-GaN, our DFT-GGA based calculations show lower band gap in comparison to the experimental data[4,14] whereas the B3LYP value is closer to the experimental investigations and other data[6,11]. Our DFT based band gaps are found to be in good agreement with theoretical values as reported earlier[9,18].

Table 1 — Measurement summary of experimental Compton profile of WZ-GaN

Sample diameter (thickness) in cm	Bulk density (g/cm^3)	Exposure time (h)	Integrated counts ($\times10^7$)	Multiple scattering (–10 to +10 au) (%)	Normalization of profile (0 to +7 au) (e$^-$)
2.2 (0.35)	3.05	297	1.05	11.07	16.86

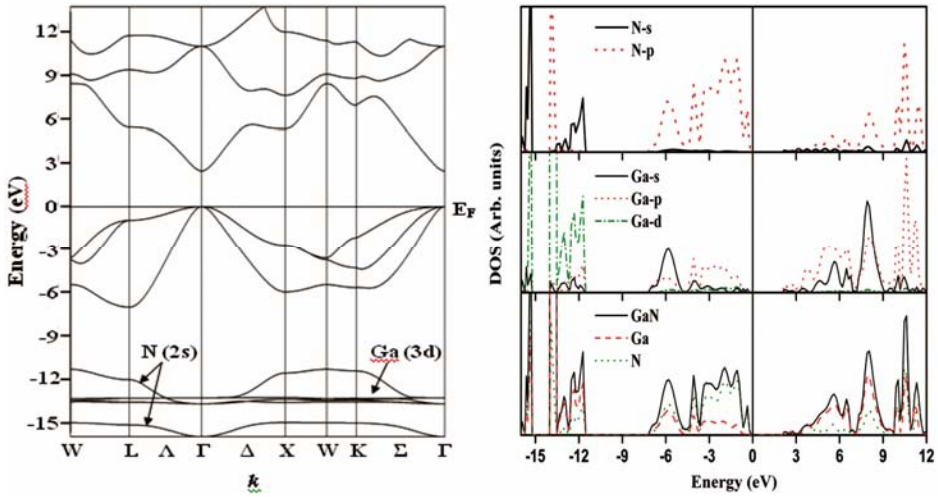

Fig. 1 — Energy bands (E-k relations) along high symmetry directions of the first Brillouin zone of ZB-GaN using GGA scheme within LCAO method. On the right hand side, the total and partial density of states (DOS) are shown

Table 2 — Calculated band gaps (ΔE_g) of GaN along with available data in eV

Method		ΔE_g	
		ZB phase	WZ phase
(i) Present work			
LCAO	DFT-LDA	2.48	2.54
	DFT-GGA	2.46	2.53
	B3LYP	3.58	4.07
(ii) Available Theory			
PP		1.6(Ref.6)	1.70(Ref.6)
GW		3.1(Ref.6)	3.50(Ref.6)
SIRC-PP		3.8(Ref.6)	4.00(Ref.6)
DFT (LDA)		2.14(Ref.18)	
DFT (LDA+U)		2.87(Ref.18)	
FP-LAPW (LDA)		1.80((Ref.19)	3.50(Ref.10)
(GGA with QP corrections)		2.4(Ref.9)	2.40(Ref.9)
FP-APW	LDA	1.93 (Ref.15)	
	GGA	1.52(Ref.15)	
PP-PW (DFT-LDA)		2.00(Ref. 5)	2.13 (Ref. 5)
		3.21(Ref.11)	3.36 (Ref.11)
(iii) Available Experiment		3.30(Ref.14)	3.41(Ref.4)
		3.21(Ref.4)	3.46 ((Ref.3)

4.1.2 WZ structure

Figure 2 shows the energy bands and DOS for the WZ-GaN. In the lowest part of valence bands (below −15.0 eV), most of the *s* character comes from N site, whereas the *d* character resides on the Ga site. Therefore, overlapping of Ga (3*d*) with the N (2*s*) states forms a particular set of bands. It is in contrast to experimental work reported earlier[3,4] wherein it is shown that the 3*d* bands lay apart from 2*s* bands. This difference can partially be explained in terms of negligence of combination of self-interaction and final screening effects in the band calculations. Our DFT calculations show that the hybridization of the N (*2p*) derived valence states enhances the effective *p-d* coupling that pushes up the valence band maximum (VBM), which leads to reduction in calculated band gap.

The VBM and the conduction band minimum (CBM) for the WZ phase is located at Γ. It indicates a direct band gap of 2.54, 2.53 and 4.07 eV for LDA, GGA and B3LYP, respectively (Table 2). Our DFT based calculations show lower band gap in comparison to the experimental data[3,4], while the B3LYP values are closer (although higher side) to the experiment. The band gap values derived from the B3LYP scheme are in very good agreement with that reported by Vogel *et al*[6]. using self-interaction and relaxation-corrections within pseudopotentials (SIRC-PP) and the DFT based values are near to those reported by other researchers[6, 11].

4.2 Compton profiles

The anisotropies in the unconvoluted Compton profiles computed from the directional profiles of ZB-and WZ-GaN within the DFT (with LDA and GGA) and the B3LYP schemes are plotted in Fig. 3(a-b). The anisotropy is calculated by taking the difference in directional Compton profiles as:

$$\Delta J(p_z) = J_{hkl}(p_z) - J_{h'k'l'}(p_z) \quad \ldots(2)$$

where [hkl] and [h′k′l′] are the principal crystallographic directions. It is seen that in WZ phase the value of $J(p_z)$ near $p_z = 0$ is high for [100].

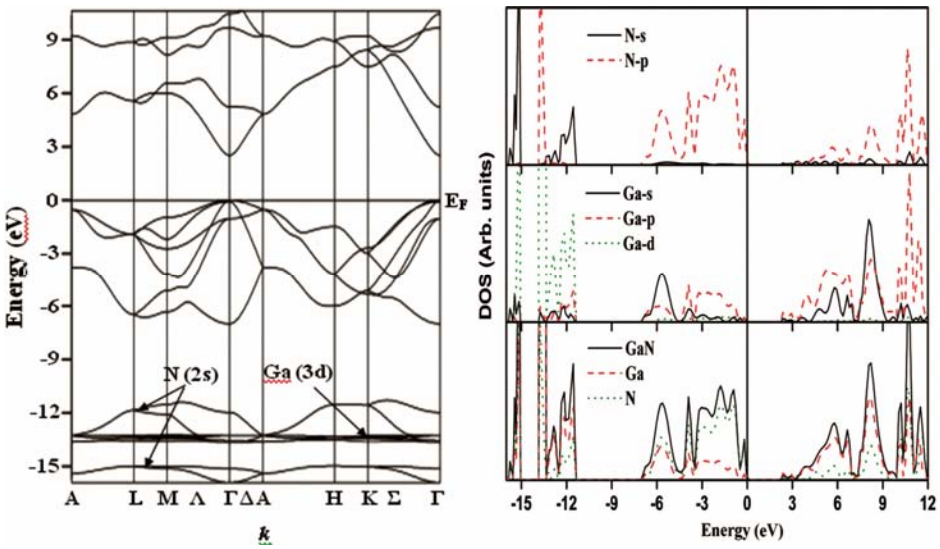

Fig. 2 — Same as Fig. 1 except the sample which is WZ-GaN

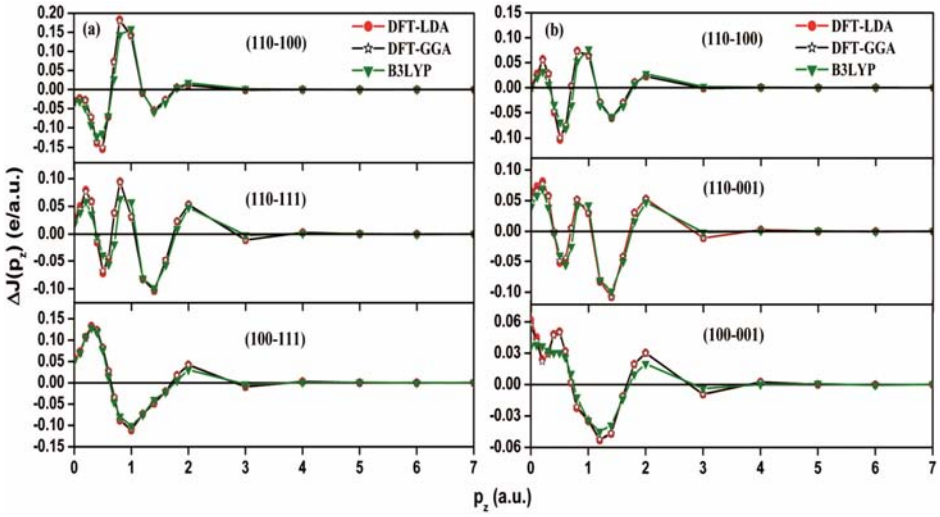

Fig. 3 — Unconvoluted anisotropies in LCAO based Compton profiles of GaN for (a) ZB phase (b) WZ phase

The numerical values of individual directional Compton profiles are available on request. The origin of anisotropy in Compton profiles can be explained on the basis of E-k relations. For example, in WZ-GaN (Fig. 2) the plane of integration normal to [100] direction contains large number of allowed states in the ΓM branch (distance ΓM = 0.602·n, n = 1, 2, 3...), which leads to higher momentum density and hence Compton profile along [100] (ΓM) direction. This tends to a negative oscillation near p_z = 0.60, 1.2 au in J_{110}–J_{100} and a positive oscillation at about 0.5 au in J_{100}–J_{001} direction as seen in Fig. 3(b).

Due to non-availability of large size single crystals (15 mm diameter and 2 mm thickness), only the isotropic experimental Compton profiles of the WZ phase (stable at room temperature) of GaN have been measured. The experimental profiles for WZ phase along with the unconvoluted theoretical values computed within the framework of the DFT (LDA and GGA) and the B3LYP are listed in Table 3.

Figure 4 shows the differences derived from convoluted theory and the experiment. All the theoretical profiles have been smeared with the instrumental resolution of 0.38 au, to account the experimental resolution. In high momentum region

Table 3 — Theoretical (unconvoluted) Compton profiles of WZ-GaN. Also included here is the isotropic experimental Compton profile of WZ-GaN. For comparison with the present experiment, all the theoretical profiles have to be convoluted with a Gaussian FWHM of 0.38 au

p_z (au)	$J(p_z)$ (e/au)			
	DFT-LDA	DFT-GGA	B3LYP	Expt.
0.0	8.173	8.154	8.122	7.560 ± 0.019
0.1	8.142	8.121	8.090	7.517
0.2	8.042	8.017	7.992	7.424
0.3	7.867	7.840	7.828	7.285
0.4	7.627	7.600	7.604	7.102
0.5	7.337	7.314	7.320	6.880
0.6	7.003	6.986	6.976	6.627
0.7	6.613	6.603	6.581	6.348
0.8	6.162	6.159	6.143	6.056
1.0	5.186	5.203	5.209	5.435 ± 0.017
1.2	4.402	4.430	4.425	4.829
1.4	3.903	3.924	3.917	4.274
1.6	3.554	3.563	3.563	3.792
1.8	3.250	3.252	3.257	3.386
2.0	2.960	2.961	2.967	3.046 ± 0.015
3.0	1.827	1.828	1.831	1.878 ± 0.011
4.0	1.156	1.155	1.159	1.171 ± 0.009
5.0	0.776	0.776	0.778	0.783 ± 0.008
6.0	0.557	0.557	0.558	0.554 ± 0.007
7.0	0.419	0.420	0.420	0.429 ± 0.004

($p_z \geq 4$ au), the theoretical profiles show a good agreement with the experimental data. It is understandable because this region is dominated by core electrons, which almost remain unaffected in bonding mechanism. It is also clear from Fig. 4 that the B3LYP based Compton line is relatively in better agreement with the present experiment, which is also confirmed on the basis of χ^2 fitting.

Now, the possible reasons for differences between theory and experiment in the low momentum region have been examined. The computation of Compton profiles from the momentum densities should incorporate the correlated states with average occupancies of single particle states lying between 0 and 1. While in LDA independent particle approximation, the occupation number density follows a step function (occupancies are one and zero only). As a result of normalization, this approximation pushes the momentum densities towards the low momentum region which leads to the higher value of theoretical Compton profiles in this region. Although, the diffused polarization functions in the basis-sets have been incorporated, even then further improvement in the quality of basis sets cannot be ruled out.

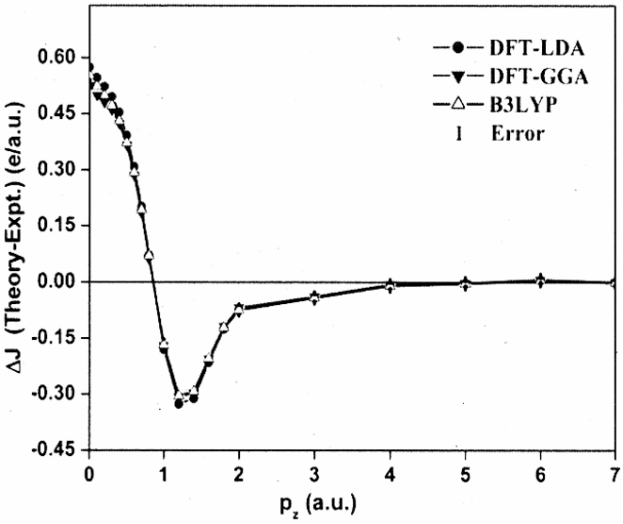

Fig. 4 — Difference between the convoluted theoretical (spherically averaged) LCAO Compton profiles and isotropic experimental profile for WZ-GaN. Solid lines are drawn

4.3 EVED profiles

To compare the relative nature of bonding in both the isoelectronic WZ-GaN and InN, the experimental profiles on p_z/p_F scale have been scaled. The scaled profiles are also known as equal-valence-electron-density (EVED) profiles. These are very promising in predicting the nature of bonding in isovalent materials[35]. The Compton profiles of WZ-InN were taken from our earlier work[21]. Figure 5(a-b) shows the normalized (4 e^-) experimental and theoretical (GGA) EVED profiles of both the WZ compounds. It is seen that the scaled experimental and theoretical $J(p_z/p_F=0)$ values for InN are lower than that of GaN. It suggests more localization of charge in the bonding direction in GaN. As a consequence, it is concluded that the WZ-GaN is more covalent than the WZ-InN, which is in agreement with the ionicity results reported by Philips[36]. In Table 4, the present atomic charge states using Mulliken's population (MP) analysis in both phases of GaN and InN are given. A similar trend of ionicity for WZ phase of both the compounds, as seen from the MP analysis in Table 4 also confirms our conclusions.

4.4 Cohesive properties

The cohesive energy of GaN can be calculated from ground state total energy of the crystalline solids (E_{GaN}^{Total}) using the following relation:

$$E_{GaN}^{Cohesive} = -E_{GaN}^{Total} + E_{Ga}^{FA} + E_{N}^{FA} \quad ...(3)$$

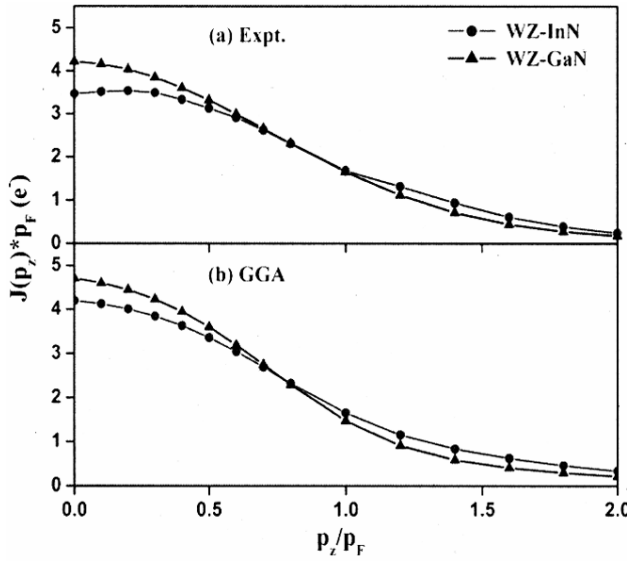

Fig. 5 — Equal-valence-electron-density (EVED) experimental and theoretical profiles (on p_z/p_F scale) of isoelectronic compounds WZ-GaN and InN. In experiment, the statistical errors are within the size of symbols used. The data for InN is taken from Sharma and Ahuja[21].

Table 4 — Atomic charge states of ZB-and WZ-GaN (in |*e*|) computed using Mulliken's population analysis employing LCAO method

Method	ZB	WZ
DFT-LDA	1.06	1.15
DFT-GGA	1.11	1.19
B3LYP	1.16	1.25

where E_{Ga}^{FA} and E_{N}^{FA} are the free atom (FA) energies corresponding to Ga and N. In such computations, the choice of atomic reference energy leads to a controversial values[25] of $E_{GaN}^{Cohesive}$. To avoid this situation, the theoretical band structure based Compton profiles and the experimental Compton profiles for the evaluation of cohesive energy, $E^{Cohesive}$, have been used. The cohesive energy can be calculated using the following relation[37,38]:

$$E^{Cohesive} = \int_0^{p_{max}} p_z^2 [J_S(p_z) - J_{FA}(p_z)]\, dp_z \qquad \ldots(4)$$

where the $J_S(p_z)$ and $J_{FA}(p_z)$ refer to solid and free atom Compton profiles of materials (presently GaN), respectively. The value of p_{max} was taken to be 2 au because after this value the $J_S(p_z)$ was almost equal to $J_{FA}(p_z)$. Further, the core contribution eliminates in the difference $J_S(p_z) - J_{FA}(p_z)$. In addition, the smallest possible value of the p_{max} reduces the experimental error arising due to multiplication of p_z^2 in the high momentum[37,38] tail as governed from Eq. (4). The values of $E^{Cohesive}$ for GaN along with the available experimental and theoretical data are listed in Table 5.

Table 5 — Cohesive energy ($E^{Cohesive}$) of GaN in eV along with the results of other investigations

Method	ZB phase	WZ phase
(i) Present work		
LCAO-DFT-LDA	10.29	8.91
LCAO-DFT-GGA	10.63	9.15
LCAO-B3LYP	10.28	9.10
Compton Expt.		8.92 ± 0.03
(ii) Available theory		
(a) PPPW-LDA	10.54[5]	10.55[5]
	10.18[8]	10.19[8]
(b) PPPW-GGA	8.25[8]	8.27[8]
(c) PP-LDA	10.68[12]	
(d) LAPW-LDA	10.80[12]	
(e) PP-PBE	8.74[12]	
(f) FPLAPW-PBE	8.86[12]	
(iii) Available Expt	8.96[2]	9.06[7, 8]

PP-PBE: pseudopotential with Perdew-Burke-Ernzerhof potentials
AE: all-electron

It can be seen that the $E^{Cohesive}$ for ZB-GaN calculated from various approximations of the LCAO method is comparable to other reported values[5,8,12] using various approaches, but differ from the PP and LAPW calculations using the PBE approximation[12] and the available experiment[2]. In case of the WZ-GaN, the present data agree with the present experimental data and other available theoretical and experimental data[7,8].

Our experimental and theoretical values of the $E^{Cohesive}$ suggest that the Compton profile measurements on such type of materials can be used for the computation of cohesive energy, a limitation may be a careful choice of the p_{max} in the integral given in Eq. (4).

5 Conclusions

The energy bands and DOS of the ZB and WZ phases of GaN are presented. The values of band gaps derived from the hybridization of HF and DFT schemes (so called B3LYP) are close to the available experimental data. The B3LYP based Compton profiles for the WZ phases are found to be relatively

in better agreement with the experimental values. Using the EVED profiles and the Mulliken's population analysis, it is concluded that InN is more ionic (or less covalent) than GaN. The present experimental and theoretical cohesive energies of GaN, which are based on Compton spectroscopy and hence free from choice of atomic reference energy, are consistent with the earlier data. The present work establishes a trend setting methodology for computation of cohesive energy using electron momentum densities.

Acknowledgement

The authors are thankful to Department of Science Technology (DST), New Delhi and DST-FIST for financial support. We are grateful to Prof R Dovesi for providing the CRYSTAL03 code.

References

1 Cooper M J, Mijnarends P E, Shiotani N *et al.*, *X-ray Compton Scattering,* Oxford Science Publications, New York, 2004.
2 Gil B, *Group III Nitride Semiconductor Compounds: Physics and Applications* Oxford University Press, Oxford, 1998; also: Harrison W A, *Electronic Structure and the Properties of Solids,* Dovor, New York, 1989.
3 Perlin P, Gorczyca I, Christensen N E *et al.*, *Phys Rev B,* 45 (1992) 13307.
4 Powell R C, Lee N E, Kim Y W & Greene J E, *J Appl Phys*, 73 (1993) 189.
5 Satta A, Fiorentini V, Bosin A & Meloni F *Gallium Nitride and Related Materials* MRS Symposia Proceedings, Materials Research Society, Pittsburgh, 1996
6 Vogel D, Kruger P & Pollmann J, *Phys Rev B,* 55 (1997) 12836.
7 Paulus B, Shi F-J & Stoll H, *J Phys-Condens Matter*, 9 (1997) 2745.
8 Stampfl C & Van de Walle C G, *Phys Rev B,* 59 (1999) 5521.
9 Gavrilenko V I & Wu R Q, *Phys Rev B*, 61 (2000) 2632.
10 Abbar B, Bouhafs B, Aourag H *et al*, *Phys Status Solidi B*, 228 (2001) 457.
11 Wang S Q & Ye H Q, *J Phys: Condens Matter*, 14 (2002) 9579.
12 Fuchs M, Da Silva J L F, Stampfl C *et al*, *Phys Rev B,* 65 (2002) 245212.
13 Vurgaftman I & Meyer J R, *J Appl Phys*,94 (2003) 3675 and reference therein.
14 Mmarques M, Teles L K, Scolfaro L M R & Leite J R, *Appl Phys Lett*, 83 (2003) 890.
15 Kanoun M B, Goumri-Said S, Merad A E *et al*, *Semicond Sci Technol*, 19 (2044) 1220.
16 Li S & Ouyang C, *Phys Lett A*, 336 (2005) 145.
17 Rosa A L & Neugebauer J, *Phys Rev B*, 73 (2006) 205346.
18 Janotti A, Segev D & Van de Walle C G, *Phys Rev B*, 74 (2006) 045202.
19 Berrah S, Boukortt A & Abid H, *Phys Scr*,75 (2007) 414.
20 Rinke P, Winkelnkemper M, Qteish A *et al*, *Phys Rev B*, 77 (2008) 075202 and reference therein
21 Sharma V & Ahuja B L, *Phys Lett A*, 372, (2008) 5377.
22 Dong L, Yadav S K, Ramprasad R & Alpay S P, *Appl Phys Lett*, 96 (2010) 202106.
23 Du Y, Chang B, Fu X *et al.*, *Optik*,123 (2012) 2208.
24 Qin L, Duan Y, Shi H *et al.*, *J Phys: Condens Matter,* 25 (2013) 045801.
25 Saunders V R, Dovesi R, Roetti C *et al*, *CRYSTAL2003 User's Manual*, University of Torino, Torino, 2003.
26 Von Barth U & Hedin L, *J Phys C: Solid State Phys,* 5 (1972) 1629.
27 Perdew J P, Burke K & Ernzerhof M, *Phys Rev Lett*, 77 (1996) 3865.
28 Becke A D, *Phys Rev A,* 38 (1988) 3098.
29 Lee C, Yang W & Parr R G, *Phys Rev B*, 37 (1988) 785.
30 Vosko S H, Wilk L & Nusair M, *Can J Phys*, 58 (1980) 1200.
31 http://wwwtcmphycamacuk/~mdt26/basis_sets
32 Johnson D D, *Phys Rev B*, 38 (1988) 12807.
33 Wright A F & Nelson J S, *Phys Rev B,* 51 (1995) 7866.
34 Ahuja B L, Sharma M & Mathur S, *Nucl Instr Meth B,* 244 (2006) 419.
35 Pandya R K, Joshi K B, Jain R *et al*, *Phys Status Solidi (b)*, 200 (1994) 137.
36 Philips J C, *Rev Mod Phys,* 42 (1970) 317.
37 Holt R S & Cooper M J, *Philos Mag B*, 41 (1980) 117.
38 Mittal U, Sharma B K, Mohammad F M & Ahuja B L, *Phys Rev B*, 38 (1988) 12208.